Draft version April 22, 2026
Typeset using LaTeX **twocolumn** style in AASTeX7

What is Powering the Enigmatic He II Emitter *Hebe*: The First Stars or Black Holes?

Junehyoung Jeon,[1,2,*] Tae Bong Jeong,[1,2,*] Saiyang Zhang (張賽暘),[2,3,4,*] and Volker Bromm[1,2,4]

[1] *Department of Astronomy, University of Texas, Austin, TX 78712, USA*
[2] *Cosmic Frontier Center, The University of Texas at Austin, Austin, TX 78712, USA*
[3] *Department of Physics, University of Texas at Austin, Austin, TX 78712, USA*
[4] *Weinberg Institute for Theoretical Physics, University of Texas, Austin, TX 78712, USA*

ABSTRACT

Recent high-resolution spectroscopy with the James Webb Space Telescope (JWST) has confirmed the presence of a strong He II λ1640 emitting clump in the vicinity of GN-z11, with only upper limits on its metallicity. To explain the peculiar properties of this source, now termed *Hebe*, a cluster of metal-free, Population III (Pop III) stars has been invoked. A less likely source for the hard UV ionizing radiation could be an accreting supermassive black hole (SMBH) embedded inside *Hebe*. We here provide further constraints on what could power the observed emission lines in *Hebe*. Comparing with cosmological simulations of Pop III star cluster formation, we assess the maximum Pop III stellar mass that could plausibly form at the location of *Hebe*, finding stellar masses of a few $10^5\,M_\odot$, consistent with those inferred from the observations. Modeling the continuum spectral energy distribution arising from an accreting SMBH, we derive He II and H I ionizing rates and the resulting recombination line luminosities, roughly in line with the observations. We thus confirm the interpretation of *Hebe* as a remarkable, primordial object, with the most plausible power source provided by a massive cluster of Pop III stars, at the limit of what is allowed within the standard model of first star formation.

Keywords: Early universe — Supermassive black holes — Population III stars — Theoretical models

1. INTRODUCTION

The pursuit of Population III (Pop III), the first generation of metal-free stars, is compelling (e.g., H. E. Bond 1981; V. Bromm & R. B. Larson 2004; V. Bromm 2013; R. S. Klessen & S. C. O. Glover 2023), given the intricate connection to cold dark matter (CDM)-driven cosmological structure formation (e.g., H. M. P. Couchman & M. J. Rees 1986; M. Tegmark et al. 1997). However, Pop III stars have remained elusive, both at high-redshifts (e.g., A. T. P. Schauer et al. 2020), and during extensive, 'stellar-archaeological' surveys of the Local Group (e.g., T. C. Beers & N. Christlieb 2005; T. Hartwig et al. 2015). With the launch of the James Webb Space Telescope (JWST), the search for Pop III has entered a new phase, focused on possible 'late-forming' systems during the epoch of reionization (B. Liu & V. Bromm 2020; A. Venditti et al. 2023; S. Fujimoto et al. 2025).

Email: junehyoungjeon@utexas.edu
* These authors contributed equally to this work.

The main challenge for such late Pop III star formation is the rapid chemical enrichment, predicted in the wake of the first supernovae, establishing a 'bedrock' metallicity of $\sim 1\%$ solar within the first galaxies (e.g., A. Pallottini et al. 2014; J. Jaacks et al. 2018). Early JWST surveys have confirmed this prediction, based on extensive spectroscopic follow-up (e.g., K. Nakajima et al. 2023), out to the highest redshifts, $z \gtrsim 12$, reached so far (e.g., F. D'Eugenio et al. 2024). Due to the highly inhomogeneous nature of early metal enrichment, driven by turbulent transport processes (e.g., A. P. Ji et al. 2015; J. Mead et al. 2025), pockets of pristine gas may survive until $z \sim 5$, at the tail-end of the probability distribution. The recently discovered AMORE6 galaxy at $z \simeq 5.7$ is a promising candidate, with tight upper limits on its metal content of $\lesssim 0.1\%$ solar (T. Morishita et al. 2025). The strongly lensing-magnified LAP1 system exhibits similar characteristics at even higher redshifts of $z \simeq 6.6$, including multiple hydrogen Lyman and Balmer line detections (E. Vanzella et al. 2023). The key question is whether such pockets could host Pop III star formation that is sufficiently massive, and therefore lu-

minous enough, to be observable with JWST (e.g., T. B. Jeong et al. 2026).

Due to the high photospheric temperatures predicted for Pop III stars ($\lesssim 10^5$ K), a key signature of metal-free star formation is the presence of strong He II emission lines (e.g., J. Tumlinson & J. M. Shull 2000; V. Bromm et al. 2001; S. P. Oh et al. 2001; D. Schaerer 2002; J. L. Johnson et al. 2009). With JWST, such He II emitters powered by Pop III may finally have come within reach (e.g., K. Nakajima & R. Maiolino 2022; A. Venditti et al. 2024, 2026; H. Katz et al. 2025). Indeed, a promising candidate for a surviving Pop III pocket was recently discovered close to the luminous GN-z11 galaxy at $z = 10.6$, initially observed only through its strong He II emission, with only upper limits on the continuum and any metal lines (R. Maiolino et al. 2024a). Based on deep JWST integral-field spectroscopy, this identification has been confirmed, also with the additional detection of hydrogen Hγ emission (R. Maiolino et al. 2026; H. Übler et al. 2026).

What is powering this remarkable source, now termed *Hebe* by R. Maiolino et al. (2026)? These authors suggest a Pop III star cluster as the most plausible explanation, using the observations to place constraints on the primordial initial mass function (IMF; E. Rusta et al. 2026), but also discuss accreting supermassive black holes (SMBHs) as alternatives. We here revisit the physical nature of *Hebe*, constraining the Pop III stellar mass that could plausibly form in the vicinity of GN-z11, based on cosmological simulations of Pop III star forming systems. Such independent constraint can help break the degeneracies in the analysis of E. Rusta et al. (2026). For completeness, we also assess the plausibility of a SMBH power source inside *Hebe*, exploring both direct-collapse and primordial black hole (BH) scenarios.

2. THEORETICAL MODELS

We investigate two main scenarios to explain *Hebe*: A Pop III star cluster or an accreting SMBH, arising from a heavy-seed pathway (e.g., A. Smith & V. Bromm 2019; K. Inayoshi et al. 2020). Both sources could provide large amounts of hard UV-ionizing radiation to produce the observed He II emission. For the flat ΛCDM cosmological parameters, we adopt a matter density of $\Omega_{\rm m} = 1 - \Omega_\Lambda = 0.315$, baryon density $\Omega_{\rm b} = 0.048$, $h = 0.6774$, and normalization parameter $\sigma_8 = 0.829$ (Planck Collaboration et al. 2016).

2.1. *Population III Star Cluster*

Previous studies have shown that a Pop III stellar system could produce strong He II line emission ($L_{\rm HeII\lambda1640} \geq 10^{40}$ erg s^{-1}) to match *Hebe* (R. Maiolino et al. 2026; A. Venditti et al. 2026). We therefore further investigate this scenario, under the assumption that *Hebe* is hosting a Pop III star cluster.

Multiple physical processes can influence the mass of the Pop III starburst. Dominant among them is the strong radiation feedback from nearby sources, especially via photons in the Lyman-Werner (LW) band (e.g., E. Visbal et al. 2017; K. Sugimura et al. 2024; T. B. Jeong et al. 2026). For example, T. B. Jeong et al. (2026) showed a significant correlation between the Pop III starburst mass and the strength of the local LW flux, with a maximum of $M_{\star,\rm Pop\ III} \approx 10^6\ M_\odot$. This limiting stellar mass is possibly realized when the galaxy reaches a dynamical mass of $M_{\rm vir} \approx 10^8\ M_\odot$, resulting in a strong starburst on short timescales ($\Delta t \lesssim 5$ Myr). Here, we explore GN-z11 as the source of the LW flux that is irradiating the *Hebe* clump, located at a measured distance of ~ 3 pkpc (R. Maiolino et al. 2026).

2.1.1. *LW flux from GN-z11*

When estimating the LW flux from GN-z11 that reaches *Hebe*, we adopt an idealized analytic approach, as follows. With the distance between GN-z11 and *Hebe* fixed at $d \sim 3$ pkpc, we model the density of the intervening intergalactic medium (IGM) as $\rho_{\rm IGM} = \Omega_{\rm b}\rho_{c,0}(1+z)^3$, and assume an IGM molecular hydrogen fraction of $f_{\rm H_2} = 10^{-6}$ (D. Galli & F. Palla 2013). Following the usual custom, we normalize the LW flux, $J_{\rm LW}$, to $J_{21} = 10^{-21}$ erg s^{-1} cm^{-2} Hz^{-1} sr^{-1}. We calculate the average spectral luminosity, $\langle L_\nu \rangle$, in the LW waveband ($h\nu = 11.2 - 13.6$eV) using BPASS (J. J. Eldridge et al. 2017), for a simple stellar population (SSP), adopting stellar properties inferred for GN-z11: $M_\star = (5.6 \pm 0.6) \times 10^8 M_\odot$, $t_{\rm age} = 21 \pm 3$ Myr (A. Crespo Gómez et al. 2026).

The resulting LW flux in the vicinity of GN-z11 is

$$J_{\rm LW,GN-z11} = \frac{1}{4\pi}\frac{f_{\rm esc,LW}\langle L_\nu \rangle}{4\pi d^2 J_{21}} = \frac{f_{\rm esc,LW}}{(4\pi d)^2 \Delta\nu J_{21}} \int_{\nu_{\rm min}}^{\nu_{\rm max}} L_\nu d\nu \approx 1.9 \times 10^3, \quad (1)$$

where $\Delta\nu = \nu_{\rm max} - \nu_{\rm min}$, and $f_{\rm esc,LW}$ is the escape fraction of LW photons from GN-z11. We choose $f_{\rm esc,LW} = 0.64$, the conservative estimate from A. T. P. Schauer et al. (2017) for H and H_2 shielding, while adopting a Kroupa IMF for the metal-enriched Population II (Pop II) stellar content in GN-z11.

We estimate the self-shielding effect from H_2 in the IGM between GN-z11 and *Hebe* with the prescription in

J. Wolcott-Green et al. (2011):

$$f_{\rm shield}(N_{\rm H_2}, T) = \frac{0.965}{(1+x/b_5)^{\alpha}} + \frac{0.035}{(1+x)^{0.5}} \times \exp\left[-8.5\times10^{-4}(1+x)^{0.5}\right], \quad (2)$$

where $x \equiv N_{\rm H_2}/5\times10^{14}\,{\rm cm^{-2}}$, and $N_{\rm H_2}$ is the molecular hydrogen column density. In this equation, $b_5 \equiv b/10^5\,{\rm cm\,s^{-1}}$, where $b \equiv \sqrt{k_B T/m_{\rm H}}$ is the Doppler broadening parameter, and $\alpha = 1.1$. The column density of molecular hydrogen is approximately

$$N_{\rm H_2} = \frac{f_{\rm H_2}\times\rho_{\rm IGM}\times0.752}{2m_{\rm H}}\times d \approx 10^{12}\,{\rm cm^{-2}}. \quad (3)$$

Here, we assume that the IGM temperature is fixed at $T = 10^3\,{\rm K}$, representing the volume-average at mean density (E. Garaldi et al. 2022). We have neglected the HI-shielding effect due to Lyman series absorption in the IGM (Z. Haiman et al. 2000), as it would become significant only at $N_{\rm H} \gtrsim 10^{22}\,{\rm cm^{-2}}$ (e.g., M. Neyer & J. Wolcott-Green 2022). Therefore, the effective $J_{\rm LW}$ experienced by *Hebe* is

$$J_{\rm LW,eff} = f_{\rm shield}(N_{\rm H_2}, T)\times J_{\rm LW,GN-z11} \sim 1,800. \quad (4)$$

We cross-check this estimate by investigating the merger history of the combined GN-z11 and *Hebe* system, using the semi-analytic model (SAM) A-SLOTH (T. Hartwig et al. 2022, 2024; M. Magg et al. 2022). The detailed star formation and LW prescriptions can be found in previous works (B. Liu et al. 2024; J. Jeon et al. 2025b). Within the SAM, we represent the global LW background with an idealized model as (T. H. Greif & V. Bromm 2006; T. Hartwig et al. 2022):

$$J_{LW,\rm global}/J_{21} = 10^{2-z/5}\ . \quad (5)$$

To calculate the local LW flux for a given halo in the merger tree, we determine the LW photon production rate based on the total mass of active massive stars (> 5 $M_\odot$) using the fitting formula from Y. Deng et al. (2024, equ. 8). We assume that the high-mass stars are located on average at a distance of 3 pkpc, matching the distance between GN-z11 and *Hebe*. The sum of the global and local LW components is the total LW flux for the halo.

Fig. 1 shows the resulting distribution of halo masses vs. LW flux for 100 merger trees of halos between 2×10^{11} $M_\odot$ – 2×10^{12} $M_\odot$ at $z = 9$. These parameters for our target halos provide an approximate representation of the biased (overmassive) environment of GN-z11 (J. Scholtz et al. 2024). We find that halos with the inferred mass of the GN-z11 host, $\sim 2\times10^{10}$ $M_\odot$ (J. Scholtz et al. 2024), can produce the LW flux as

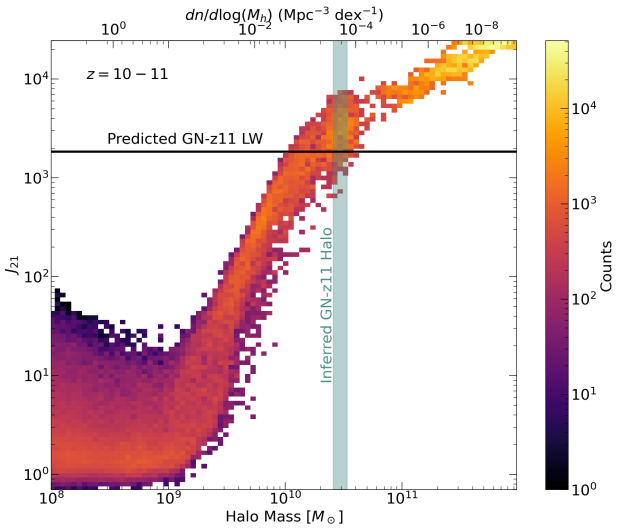

Figure 1. LW fluxes within the Lagrangian volumes of biased halos at $z = 9$, derived from A-SLOTH merger trees. We show the distribution drawn from the $z = 10-11$ time slice, and for comparison mark the LW flux from GN-z11 as predicted above (Sec. 2.1.1), together with its inferred halo mass (J. Scholtz et al. 2024). We also reproduce halo number densities from the GUREFT mass function (L. Y. A. Yung et al. 2024), indicating that halos able to produce such high LW fluxes are rare ($\sim 10^{-4}$ Mpc^{-3} dex^{-1}), while still being within reach of current JWST surveys.

estimated above, thus further supporting our overall argument here. We note that, based on the GUREFT halo mass function (L. Y. A. Yung et al. 2024), the number densities of such GN-z11-like systems are low ($\sim 10^{-4}$ Mpc^{-3} dex^{-1}), but still within reach of current JWST surveys (with effective survey volumes at $z \sim 10$ of $\sim 10^5$ Mpc^3; see, e.g., A. Venditti et al. 2024).

2.1.2. *Pop III Starburst Mass Prediction*

From the estimated effective LW flux for GN-z11 ($J_{\rm LW,eff}$) in Section 2.1.1, we can constrain the Pop III starburst mass of *Hebe*. Using simulated results from T. B. Jeong et al. (2026), we derive the following fitting formula for the Pop III starburst mass as a function of the LW flux,

$$\log M_{\star,\rm Pop\ III}(J_{\rm LW}) = \frac{b}{(1 + a\times\exp(-2k\log J_{\rm LW}))} + c, \quad (6)$$

where a, b, c, and k are free parameters. We evaluate the fit for two phases, the initial starburst phase ($\langle t_{\rm age}\rangle \simeq 1.5\,{\rm Myr}$), and the time when the Pop III starburst mass is maximized ($\langle t_{\rm age}\rangle \lesssim 2.5\,{\rm Myr}$).

As can be seen in Fig. 2, we infer that the Pop III starburst mass in *Hebe* (yellow stars) is $M_{\star,\rm Pop\ III} \sim 2.5\times10^5\ M_\odot$ for the initial Pop III starburst, and $M_{\star,\rm Pop\ III} \sim 6.6\times10^5\ M_\odot$ when the maximum mass

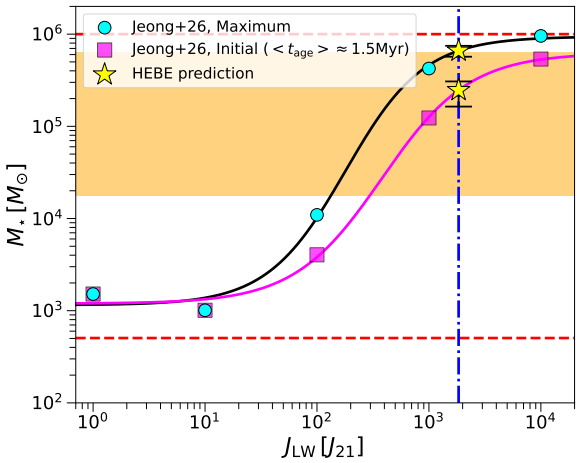

Figure 2. Pop III starburst mass vs. strength of LW flux. We reproduce the results from the cosmological simulation in T. B. Jeong et al. (2026), showing the initial Pop III starburst phase ($\langle t_{\rm age}\rangle \simeq 1.5$ Myr) with magenta squares, and the time when the maximum Pop III mass is reached ($\langle t_{\rm age}\rangle \lesssim 2.5$Myr) with cyan circles, together with the fitting results (black and magenta solid lines). We mark the Pop III starburst mass predicted for *Hebe* with yellow-star symbols (including 1σ error bars), based on the estimated LW flux (blue dash-dotted line). The orange shaded region indicates the mass range for *Hebe*, as estimated in E. Rusta et al. (2026).

is attained. These results are fully consistent with the results in E. Rusta et al. (2026), which suggest a total stellar mass for *Hebe* in the range of $10^{4.25}\ M_\odot \leq M_\star \leq 10^{5.8}\ M_\odot$ at $t_{\rm age} = 2$ Myr, depending on the functional form of the Pop III IMF.

2.2. *Supermassive Black Holes*

Another scenario for *Hebe* is that the He II emission originates from an accreting SMBH. However, any such SMBH origin is severely constrained by the observed narrow line widths, implying central BH masses of $M_\bullet \lesssim 10^4 M_\odot$ (R. Maiolino et al. 2026). For completeness, we here further consider the plausibility of the SMBH alternative, focusing on heavy-seed pathways[5], such as a direct-collapse black hole (DCBH) or a primordial black hole (PBH).

2.2.1. *BH Seed Formation*

The DCBH pathway is based on the runaway collapse of a massive, extremely metal-poor ($Z \lesssim 10^{-3}$ $Z_\odot$; S. Chon & K. Omukai 2024) gas cloud, involving a supermassive star (SMS) as an intermediate, short-lived stage (e.g., V. Bromm & A. Loeb 2003; M. C. Begelman et al. 2006; G. Lodato & P. Natarajan 2006). This channel produces a more massive BH seed ($\sim 10^4 - 10^6$ $M_\odot$; F. Becerra et al. 2018), and requires rare conditions that suppress low-temperature gas cooling mechanisms, such as a nearby stellar population providing LW radiation that destroys molecular hydrogen, allowing the cloud to collapse without fragmenting into a large number of ordinary/low-mass stars (e.g., J. L. Johnson et al. 2013; J. H. Wise et al. 2019; L. Haemmerlé et al. 2018, 2020). Thus, DCBHs are initially expected to form without a host stellar population, but separate from it.

Another pathway invokes PBHs, theorized to form shortly after the Big Bang from the collapse of primordial overdensities and could span a broad range of masses, including those relevant for heavy BH seeds ($\gtrsim 10^4$ $M_\odot$; Y. B. Zel'dovich & I. D. Novikov 1967; S. Hawking 1971; B. J. Carr 1975; K. M. Belotsky et al. 2019; A. Escrivà 2022). Unlike the DCBH channel, the PBH scenario does not rely on a pre-existing star-forming environment. Instead, PBHs may begin to influence their surroundings at very early times. In particular, efficient radiative feedback from PBH accretion can suppress gas cooling, hinder fragmentation, and delay or regulate the onset of star formation (see e.g., B. Liu et al. 2022; S. Zhang et al. 2025). This may naturally lead to a configuration in which BH growth precedes, or is at least partially decoupled from, the assembly of a nearby stellar structure like GN-z11.

Both pathways can produce a system where the main stellar population, analogous to GN-z11, is separate from the He II emitter, here assumed to be powered by an embedded SMBH. In Fig. 3, we show an example of such a configuration for the DCBH pathway, reproduced from the numerical simulations in J. Jeon et al. (2025a). The DCBH initially forms in a metal-poor dark matter halo with low stellar mass, but soon merges with a different halo, which had formed a massive stellar population with the corresponding supernova enrichment. As metal enrichment is highly inhomogeneous in the early Universe (e.g., A. Pallottini et al. 2014; J. Jaacks et al. 2019), such disparate regions can exist in relatively close proximity. Fully addressing this intricate, multi-scale metal-transport problem requires dedicated follow-up simulations, and is beyond the scope of our exploratory study here.

2.2.2. *SMBH SED Modeling*

Regardless of its specific origin, we next assess whether an accreting SMBH could power the line emission ob-

[5] The metallicity and timing constraints for *Hebe* effectively exclude models where a light, stellar-remnant, seed would grow via rapid accretion.

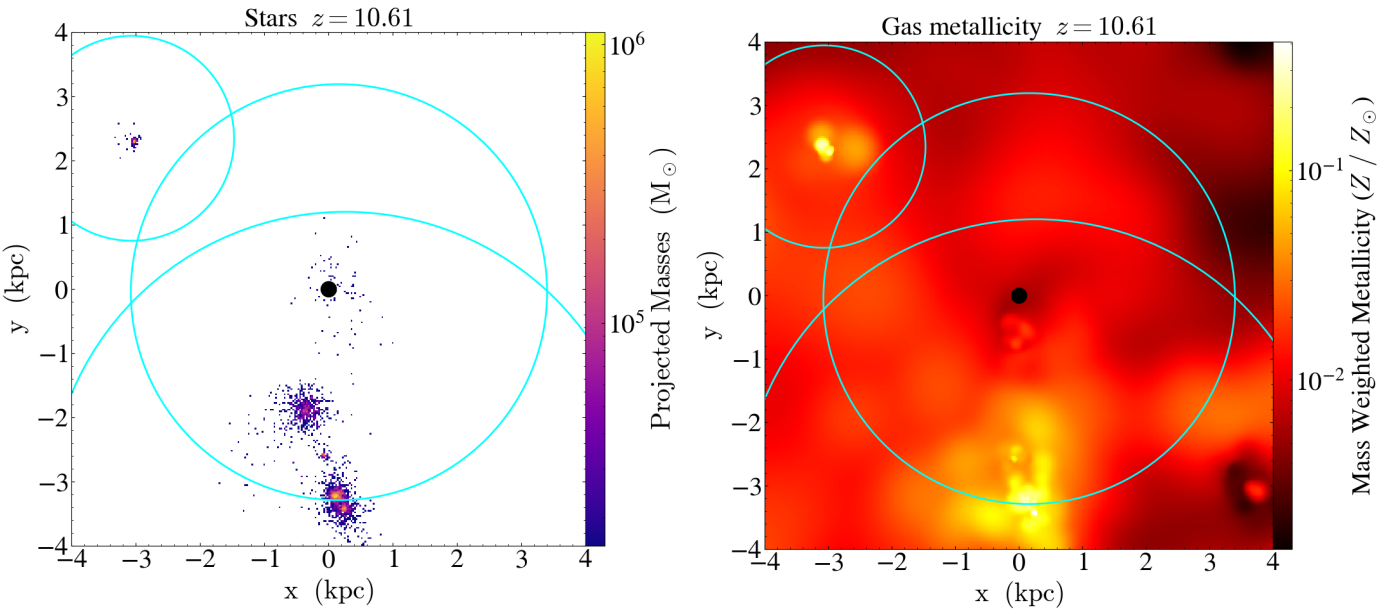

Figure 3. Example of a heavy-seed BH located close to a massive stellar dominated system, taken from the simulation suite in J. Jeon et al. (2025a). This configuration is analogous to GN-z11 and *Hebe* within the SMBH scenario. We show the stellar mass (*left*) and metallicity (*right*) in projection, with dark matter host halos ($\sim 10^8 - 10^9$ $M_\odot$) indicated as cyan circles. As can be seen, the main stellar component is separated by ~ 3 pkpc from the SMBH, marked as a black dot. The simulated SMBH has a mass of $\sim 10^6$ $M_\odot$ originating from a DCBH, and experiencing some subsequent growth. The actual *Hebe* system may originate from a similar configuration, but with less efficient SMBH growth (e.g., J. Jeon et al. 2023), where a DCBH or a PBH initially forms in a metal-poor environment, and merges with a nearby metal-enriched stellar system formed separately.

served in *Hebe*. We model the BH spectral energy distribution (SED) based on the prescription in V. Takhistov et al. (2022), and derive the corresponding emission-line strengths.

Given a BH of mass $M_\bullet$ embedded in gas of hydrogen number density $n_{\rm H}$, we estimate the accretion rate using a Bondi-like prescription,

$$\dot{M}_\bullet = \frac{4\pi\,(G M_\bullet)^2\,\rho_{\rm gas}}{\tilde{v}^3}\,, \tag{7}$$

where $\rho_{\rm gas} = \mu\, m_p\, n_{\rm H}$ is the local gas mass density with mean molecular weight $\mu = 1.22$ appropriate for neutral primordial gas, and $\tilde{v}$ is the effective relative velocity between the BH and the surrounding medium. We take $\tilde{v}$ to be of order the virial velocity in an atomic cooling halo,

$$\tilde{v} \simeq \sqrt{\frac{G M_{\rm h}}{R_{\rm vir}}} \simeq 18.1\ {\rm km\,s^{-1}} \left(\frac{M_{\rm h}}{10^8\,M_\odot}\right)^{1/3} \left(\frac{1+z}{11}\right)^{1/2}. \tag{8}$$

We note that this is the dynamical mass scale inferred for *Hebe* (R. Maiolino et al. 2026). It is convenient to express the accretion rate in dimensionless form as $\dot{m} \equiv \dot{M}_\bullet / \dot{M}_{\rm Edd}$, where the Eddington accretion rate is $\dot{M}_{\rm Edd} = L_{\rm Edd}/(\epsilon_r\, c^2)$ and ϵ_r the radiative efficiency. Scaling to fiducial values gives

$$\dot{m} \simeq 0.25 \left(\frac{\epsilon_r}{0.057}\right) \left(\frac{M_\bullet}{10^4\,M_\odot}\right) \left(\frac{n_{\rm H}}{10^3\,{\rm cm^{-3}}}\right) \left(\frac{\tilde{v}}{20\,{\rm km\,s^{-1}}}\right)^{-3}. \tag{9}$$

The fiducial radiative efficiency $\epsilon_r = 0.057$ corresponds to the standard optically thick efficiency for a Schwarzschild BH. The dimensionless accretion rate $\dot{m}$, compared to the critical threshold $\dot{m}_{\rm crit} \simeq 0.07\,\alpha$, determines the structure of the accretion flow and thus the shape of the emitted spectrum, where α is the viscosity parameter and is fixed to $\alpha = 0.1$ throughout this work. For $\dot{m} > \dot{m}_{\rm crit}$, the accretion flow is assumed to be geometrically thin and optically thick, and we compute the rest-frame spectral luminosity $L_E(E)$ [erg s^{-1} eV^{-1}] using a standard multi-color disk model (N. I. Shakura & R. A. Sunyaev 1973; J. E. Pringle 1981). For $\dot{m} \le \dot{m}_{\rm crit}$, the flow becomes radiatively inefficient and advection-dominated, and we instead adopt an advection dominated accretion flow (ADAF)-like prescription (R. Narayan & I. Yi 1995). In summary,

$$L_E(E) = \begin{cases} L_E^{\rm thin}(E), & \dot{m} > \dot{m}_{\rm crit}, \\ L_E^{\rm ADAF}(E), & \dot{m} \le \dot{m}_{\rm crit}. \end{cases} \tag{10}$$

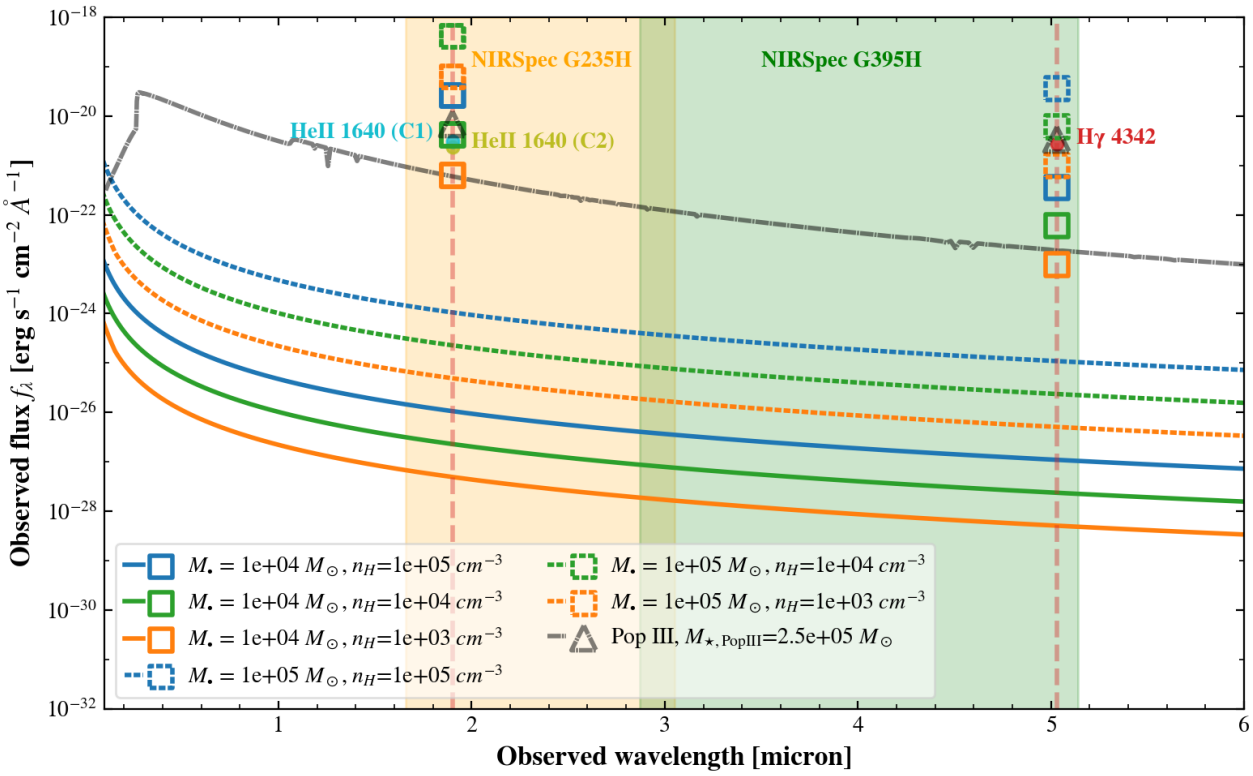

Figure 4. Observer-frame spectral energy distribution of a BH accreting at the Bondi rate within a halo of mass $M_h \sim 10^8\,M_\odot$ at $z = 10.6$, for BH masses $M_\bullet = 10^4$ and $10^5\,M_\odot$ (solid and dotted lines, respectively), and ambient densities $n_{\rm H} = 10^3$–$10^5\,{\rm cm}^{-3}$ (colors, as described in the legend). The BH rest-frame SED is modeled using the prescription from V. Takhistov et al. (2022). For comparison, we also show a Pop III simple stellar population with total stellar mass $M_{\star,\rm PopIII} = 2.5 \times 10^5\,M_\odot$ (black dot-dashed line), adopting the Yggdrasil spectral synthesis model (E. Zackrisson et al. 2011). Filled circles mark the observed line-equivalent flux densities f_λ of He II λ1640 (C1 and C2 components) and Hγ λ4342 reported by H. Übler et al. (2026); R. Maiolino et al. (2026). Open squares and triangles of matching color and line style show the predicted reprocessed line flux densities obtained by integrating the ionizing photon rate above the relevant threshold, assuming complete photon reprocessing ($f_{\rm esc} = 0$). The orange and green shaded bands indicate the wavelength coverage of the JWST/NIRSpec G235H and G395H gratings, and the vertical dashed lines mark the redshifted wavelengths of the He II λ1640 and Hγ λ4342 transitions.

In each case, $L_E(E)$ is normalized such that integration over energy recovers the bolometric luminosity $\int L_E(E)\,dE = \epsilon_r \dot{M}_\bullet c^2$.

For the low-accretion branch, the subgrid model produces a harder and more extended ionizing spectrum, intended to mimic the emission from a hot, optically thin flow. By contrast, in the thin-disk branch, the spectrum is approximated as a multicolor blackbody with an exponential high-energy cutoff, so that the emission is concentrated around the characteristic inner-disk temperature. For the parameter range relevant to *Hebe*, this branch is particularly important for setting the number of photons above the H I and He II ionization thresholds, and therefore for determining the strength of the associated recombination lines.

Once the continuum SED is specified, the rate of ionizing photons above a threshold energy E_0 follows directly from

$$Q(>E_0) = \int_{E_0}^{\infty} \frac{L_E}{E}\,dE\,, \tag{11}$$

where $E_0 = 13.6$ eV for hydrogen and 54.4 eV for singly ionized helium. In a radiation-bounded nebula where all ionizing photons are reprocessed, the luminosity of a recombination line at frequency $\nu_{\rm line}$ is

$$L_{\rm line} = (1 - f_{\rm esc})\,\epsilon_{\rm line}\,h\nu_{\rm line}\,Q\,, \tag{12}$$

where $f_{\rm esc}$ is the escape fraction and $\epsilon_{\rm line} \equiv \alpha^{\rm eff}_{\rm line}/\alpha_B$ is the fraction of recombinations that produce the line of interest (D. E. Osterbrock & G. J. Ferland 2006). Throughout this work we assume $f_{\rm esc} = 0$ for both hydrogen- and helium-ionizing photons, i.e., complete reprocessing within the nebula. For Hβ λ4861, at electron temperatures $T_e \sim 1$–3×10^4 K and densities below the collisional de-excitation limit, we adopt $\epsilon_{\rm H\beta} \approx 0.12$; higher-order Balmer lines then follow from the intrinsic

decrement, and we take $L_{\mathrm{H}\gamma}/L_{\mathrm{H}\beta} = 0.468$, appropriate for $T_e \approx 2 \times 10^4$ K. For He II λ1640, the relevant photon rate is Q_{He^+}, with an effective emission probability $\epsilon_{\mathrm{He\,II}\,1640} \approx 0.47$ at $T_e \sim 3\times10^4$ K (recombination coefficients are evaluated following P. J. Storey & D. G. Hummer 1995; V. Luridiana et al. 2015). Since the 54.4 eV threshold lies well above the hydrogen ionization edge, the ratio $Q_{\mathrm{He}^+}/Q_{\mathrm{H}}$ is sensitive to the hardness of the ionizing spectrum and therefore to the accretion state of the BH.

The resulting observer-frame fluxes are shown in Fig. 4, where we explore BH masses of 10^4 and $10^5\,M_\odot$ and ambient gas densities in the range $n_{\mathrm{H}} = 10^3$–$10^5\,\mathrm{cm}^{-3}$. The corresponding accretion rates[6] span $\dot{m} \sim 0.33$–330, covering the range from moderately sub-Eddington to hyper-Eddington. The predicted continuum level depends sensitively on both BH mass and gas density, with an overall spread of nearly four orders of magnitude, implying that observational limits on the continuum already provide a meaningful constraint on the underlying BH–gas configuration. The resulting line and continuum levels are broadly consistent with the observations reported in H. Übler et al. (2026). If part of the continuum originates from stars, models with a more modest BH-powered continuum, such as $M_{\mathrm{BH}} \sim 10^4\,M_\odot$ and $n_{\mathrm{H}} \sim 10^3$–$10^4\,\mathrm{cm}^{-3}$, are preferred because they leave room for a non-negligible stellar contribution. By contrast, models with larger M_{BH} and/or higher n_{H} tend to produce an overly dominant BH continuum. For completeness, we also show the continuum and corresponding emission-line strengths for a Pop III star cluster with the mass estimated in Section 2.1.1, indicating values that could plausibly account for the observed line fluxes. Our analysis is limited to the instantaneous configuration inferred from the data; a full reconstruction of the formation history of *Hebe* will require future high-resolution simulations.

With the same SED model, we also calculate the detectability of an accreting BH via X-ray emission. Only the most extreme models ($M_\bullet = 10^5\,M_\odot$, $n_H \geq 10^4$ cm^{-3}) produce fluxes above the Chandra Deep Field-South (CDF-S) 7 Ms limit ($\sim 1.9 \times 10^{-17}$ erg s^{-1} cm^{-2} within $0.5 - 7$ keV; B. Luo et al. 2017); the rest of the parameter space falls orders of magnitude below current X-ray sensitivity. This is not unique to *Hebe*: the broader population of JWST-discovered AGN at high redshift appears to be systematically X-ray weak (R. Maiolino et al. 2025), and even GN-z11, as a spectroscopically confirmed AGN at the same redshift and in the same field, remains X-ray undetected (R. Maiolino et al. 2024b). For comparison, the case of UHZ-1 at $z \approx 10.1$, initially reported as a $\sim 4 \times 10^7\,M_\odot$ DCBH candidate on the basis of a Chandra hard-band detection (Á. Bogdán et al. 2024; P. Natarajan et al. 2024), further illustrates these difficulties: a recent reanalysis of the full 2.2 Ms dataset finds the X-ray excess at only 2.3–2.9σ significance, while JWST/MIRI non-detections independently favor a star-forming galaxy interpretation (F. Zou et al. 2026). These examples underscore that X-ray observations at cosmic dawn alone carry little power to distinguish between accreting BH and stellar scenarios (see also J. Jeon et al. 2022). X-ray non-detection of *Hebe* is therefore consistent with, but not constraining for, most BH configurations considered here.

[6] The resulting BH rest-frame SEDs all follow the thin-disk branch in Equ. 10.

3. SUMMARY AND CONCLUSIONS

In this work, we have examined two scenarios for *Hebe*: a Pop III stellar cluster or an accreting SMBH. For the Pop III scenario, we argue that GN-z11 provides the LW flux of sufficient strength to trigger a Pop III starburst at the location of *Hebe*, with an estimated mass of $\sim 2.5 - 6.6 \times 10^5$ $\mathrm{M}_\odot$, in agreement with previous work (E. Rusta et al. 2026). For the scenario where *Hebe* is an accreting SMBH ($M_\bullet = 10^4 - 10^5$ $\mathrm{M}_\odot$), originating from a DCBH or PBH, we model the emitted continuum SED, finding that the observed *Hebe* He II and Hγ fluxes could be achieved under plausible assumptions for the SMBH mass and nearby gas density.

We note that these scenarios are not mutually exclusive. The high LW flux from GN-z11 could promote both a Pop III starburst and DCBH formation (A. Aykutalp et al. 2020; J. Jeon et al. 2025a; T. B. Jeong et al. 2026). If the SMBH mass or gas density is low enough, a combination of stellar and SMBH contributions can produce the observed *Hebe* fluxes (see Fig. 4). In any case, *Hebe* is a remarkable object, plausibly originating from the first stars, an exotic SMBH, formed from a DCBH or PBH pathway, or even a combination of both.

Observing the signatures of the first stars and SMBH seeding pathways has been a longstanding objective in astronomy, and JWST's discovery of *Hebe* marks an important milestone. Within the LW-mediated model explored here, there may be a connection to the recently discovered class of 'synchronized pairs' (E. Visbal et al. 2014), in this case UV-luminous galaxies close to Little Red Dots (LRDs), the latter assumed to host DCBH-seeded SMBHs (e.g., J. F. W. Baggen et al. 2026; J. Jeon et al. 2026; E. Cenci & M. Habouzit 2025; F. Pacucci et al. 2026). Future theoretical studies are needed to further unravel the bifurcation behavior of pristine gas clouds subject to strong LW fluxes, resulting in a mas-

sive Pop III star cluster or heavy BH seed, and future observations may provide a fuller picture of how rare *Hebe*-like objects truly are. We are entering a new, exciting phase in the pursuit of Pop III stars, and the understanding of the primordial Universe that allows them to form.

ACKNOWLEDGMENTS

The authors acknowledge the Texas Advanced Computing Center (TACC) for providing HPC resources under allocation AST23026. VB acknowledges support from the Josey Centennial Professorship in Astronomy at UT Austin.

REFERENCES

Aykutalp, A., Barrow, K. S. S., Wise, J. H., & Johnson, J. L. 2020 ApJL, 898, L53

Baggen, J. F. W., Scoggins, M. T., van Dokkum, P., et al. 2026 arXiv e-prints, arXiv:2602.02702

Becerra, F., Marinacci, F., Bromm, V., & Hernquist, L. E. 2018 MNRAS, 480, 5029

Beers, T. C., & Christlieb, N. 2005 ARA&A, 43, 531

Begelman, M. C., Volonteri, M., & Rees, M. J. 2006 MNRAS, 370, 289

Belotsky, K. M., Dokuchaev, V. I., Eroshenko, Y. N., et al. 2019 Eur. Phys. J. C, 79, 246

Bogdán, Á., Goulding, A. D., Natarajan, P., et al. 2024 Nature Astronomy, 8, 126

Bond, H. E. 1981 ApJ, 248, 606

Bromm, V. 2013 Reports on Progress in Physics, 76, 112901

Bromm, V., Kudritzki, R. P., & Loeb, A. 2001 ApJ, 552, 464

Bromm, V., & Larson, R. B. 2004 ARA&A, 42, 79

Bromm, V., & Loeb, A. 2003 ApJ, 596, 34

Carr, B. J. 1975 ApJ, 201, 1

Cenci, E., & Habouzit, M. 2025 MNRAS, 542, 2597

Chon, S., & Omukai, K. 2024 arXiv e-prints, arXiv:2412.14900

Couchman, H. M. P., & Rees, M. J. 1986 MNRAS, 221, 53

Crespo Gómez, A., Colina, L., Pérez-González, P. G., et al. 2026 A&A, 706, A46

Deng, Y., Li, H., Liu, B., et al. 2024 A&A, 691, A231

D'Eugenio, F., Maiolino, R., Carniani, S., et al. 2024 A&A, 689, A152

Eldridge, J. J., Stanway, E. R., Xiao, L., et al. 2017 PASA, 34, e058

Escrivà, A. 2022 Universe, 8, 66

Fujimoto, S., Naidu, R. P., Chisholm, J., et al. 2025 ApJ, 989, 46

Galli, D., & Palla, F. 2013 ARA&A, 51, 163

Garaldi, E., Kannan, R., Smith, A., et al. 2022 MNRAS, 512, 4909

Greif, T. H., & Bromm, V. 2006 MNRAS, 373, 128

Haemmerlé, L., Mayer, L., Klessen, R. S., et al. 2020 SSRv, 216, 48

Haemmerlé, L., Woods, T. E., Klessen, R. S., Heger, A., & Whalen, D. J. 2018 MNRAS, 474, 2757

Haiman, Z., Abel, T., & Rees, M. J. 2000 ApJ, 534, 11

Hartwig, T., Bromm, V., Klessen, R. S., & Glover, S. C. O. 2015 MNRAS, 447, 3892

Hartwig, T., Lipatova, V., Glover, S. C. O., & Klessen, R. S. 2024 MNRAS, 535, 516

Hartwig, T., Magg, M., Chen, L.-H., et al. 2022 ApJ, 936, 45

Hawking, S. 1971 Monthly Notices of the Royal Astronomical Society, 152, 75

Inayoshi, K., Visbal, E., & Haiman, Z. 2020 ARA&A, 58, 27

Jaacks, J., Finkelstein, S. L., & Bromm, V. 2019 MNRAS, 488, 2202

Jaacks, J., Thompson, R., Finkelstein, S. L., & Bromm, V. 2018 MNRAS, 475, 4396

Jeon, J., Bromm, V., & Finkelstein, S. L. 2022 MNRAS, 515, 5568

Jeon, J., Bromm, V., Liu, B., & Finkelstein, S. L. 2025a ApJ, 979, 127

Jeon, J., Liu, B., Bromm, V., & Finkelstein, S. L. 2023 MNRAS, 524, 176

Jeon, J., Liu, B., Taylor, A. J., et al. 2025b ApJ, 988, 110

Jeon, J., Liu, B., Bromm, V., et al. 2026 ApJ, 998, 148

Jeong, T. B., Venditti, A., Bromm, V., et al. 2026 arXiv e-prints, arXiv:2603.23209

Ji, A. P., Frebel, A., & Bromm, V. 2015 MNRAS, 454, 659

Johnson, J. L., Greif, T. H., Bromm, V., Klessen, R. S., & Ippolito, J. 2009 MNRAS, 399, 37

Johnson, J. L., Whalen, D. J., Li, H., & Holz, D. E. 2013 ApJ, 771, 116

Katz, H., Rey, M. P., Cadiou, C., et al. 2025 arXiv e-prints, arXiv:2510.05201

Klessen, R. S., & Glover, S. C. O. 2023 ARA&A, 61, 65

Liu, B., & Bromm, V. 2020 MNRAS, 497, 2839

Liu, B., Zhang, S., & Bromm, V. 2022 MNRAS, 514, 2376

Liu, B., Hartwig, T., Sartorio, N. S., et al. 2024 MNRAS, 534, 1634

Lodato, G., & Natarajan, P. 2006 MNRAS, 371, 1813

Luo, B., Brandt, W. N., Xue, Y. Q., et al. 2017 ApJS, 228, 2

Luridiana, V., Morisset, C., & Shaw, R. A. 2015 A&A, 573, A42
Magg, M., Hartwig, T., Chen, L.-H., & Tarumi, Y. 2022 The Journal of Open Source Software, 7, 4417
Maiolino, R., Übler, H., Perna, M., et al. 2024a A&A, 687, A67
Maiolino, R., Scholtz, J., Witstok, J., et al. 2024b Nature, 627, 59
Maiolino, R., Risaliti, G., Signorini, M., et al. 2025 MNRAS, 538, 1921
Maiolino, R., Übler, H., Perna, M., et al. 2026 arXiv e-prints, arXiv:2603.20362
Mead, J., Brauer, K., Bryan, G. L., et al. 2025 arXiv e-prints, arXiv:2509.13580
Morishita, T., Liu, Z., Stiavelli, M., et al. 2025 arXiv e-prints, arXiv:2507.10521
Nakajima, K., & Maiolino, R. 2022 MNRAS, 513, 5134
Nakajima, K., Ouchi, M., Isobe, Y., et al. 2023 ApJS, 269, 33
Narayan, R., & Yi, I. 1995 ApJ, 452, 710
Natarajan, P., Pacucci, F., Ricarte, A., et al. 2024 ApJL, 960, L1
Neyer, M., & Wolcott-Green, J. 2022 arXiv e-prints, arXiv:2210.09532
Oh, S. P., Haiman, Z., & Rees, M. J. 2001 ApJ, 553, 73
Osterbrock, D. E., & Ferland, G. J. 2006, Astrophysics of gaseous nebulae and active galactic nuclei
Pacucci, F., Ferrara, A., & Kocevski, D. D. 2026 arXiv e-prints, arXiv:2601.14368
Pallottini, A., Ferrara, A., Gallerani, S., Salvadori, S., & D'Odorico, V. 2014 MNRAS, 440, 2498
Planck Collaboration, Ade, P. A. R., Aghanim, N., et al. 2016 A&A, 594, A13
Pringle, J. E. 1981 ARA&A, 19, 137
Rusta, E., Salvadori, S., Maiolino, R., et al. 2026 arXiv e-prints, arXiv:2603.20363
Schaerer, D. 2002 A&A, 382, 28
Schauer, A. T. P., Drory, N., & Bromm, V. 2020 ApJ, 904, 145
Schauer, A. T. P., Agarwal, B., Glover, S. C. O., et al. 2017 MNRAS, 467, 2288
Scholtz, J., Witten, C., Laporte, N., et al. 2024 A&A, 687, A283
Shakura, N. I., & Sunyaev, R. A. 1973 A&A, 24, 337
Smith, A., & Bromm, V. 2019 Contemporary Physics, 60, 111
Storey, P. J., & Hummer, D. G. 1995 MNRAS, 272, 41
Sugimura, K., Ricotti, M., Park, J., Garcia, F. A. B., & Yajima, H. 2024 ApJ, 970, 14
Takhistov, V., Lu, P., Gelmini, G. B., et al. 2022 JCAP, 2022, 017
Tegmark, M., Silk, J., Rees, M. J., et al. 1997 ApJ, 474, 1
Tumlinson, J., & Shull, J. M. 2000 ApJL, 528, L65
Übler, H., Maiolino, R., Pérez-González, P. G., et al. 2026 arXiv e-prints, arXiv:2603.20360
Vanzella, E., Loiacono, F., Bergamini, P., et al. 2023 A&A, 678, A173
Venditti, A., Bromm, V., Finkelstein, S. L., et al. 2024 ApJL, 973, L12
Venditti, A., Graziani, L., Schneider, R., et al. 2023 MNRAS, 522, 3809
Venditti, A., Graziani, L., Schneider, R., et al. 2026 arXiv e-prints, arXiv:2603.27582
Visbal, E., Bryan, G. L., & Haiman, Z. 2017 MNRAS, 469, 1456
Visbal, E., Haiman, Z., & Bryan, G. L. 2014 MNRAS, 445, 1056
Wise, J. H., Regan, J. A., O'Shea, B. W., et al. 2019 Nature, 566, 85
Wolcott-Green, J., Haiman, Z., & Bryan, G. L. 2011 MNRAS, 418, 838
Yung, L. Y. A., Somerville, R. S., Nguyen, T., et al. 2024 MNRAS, 530, 4868
Zackrisson, E., Rydberg, C.-E., Schaerer, D., Östlin, G., & Tuli, M. 2011 ApJ, 740, 13
Zel'dovich, Y. B., & Novikov, I. D. 1967 Soviet Ast., 10, 602
Zhang, S., Liu, B., Bromm, V., et al. 2025 ApJ, 987, 185
Zou, F., Gallo, E., Zuo, Z., et al. 2026 arXiv e-prints, arXiv:2603.24893